Journal of
Materials Chemistry A

Accepted Manuscript

This article can be cited before page numbers have been issued, to do this please use: X. Wu, B. Wang, Z. Yang and L. Chen, *J. Mater. Chem. A*, 2019, DOI: 10.1039/C8TA11447A.

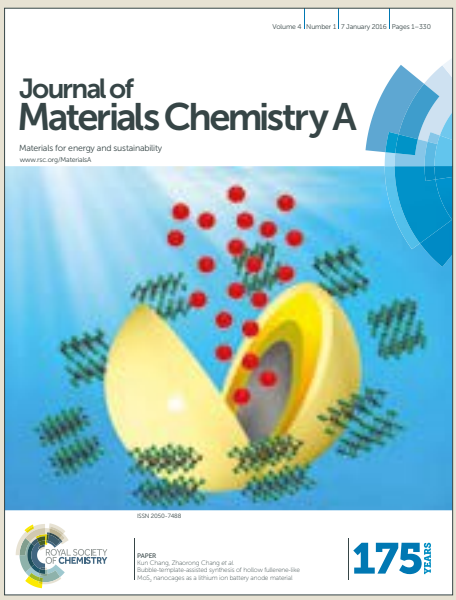

ROYAL SOCIETY OF CHEMISTRY

rsc.li/materials-a

View Article Online
DOI: 10.1039/C8TA11447A

Journal Name

ARTICLE

Novel covalent organic frameworks: preparation, characterization and application

Received 00th January 20xx,
Accepted 00th January 20xx

DOI: 10.1039/x0xx00000x

www.rsc.org/

Xingchun Wu,[a,b,1] Bowei Wang, [a,b,c,1] Ziqi Yang [a,b] and Ligong Chen [*a,b,c]

Covalent organic frameworks (COFs) have attracted considerable interest over the past few years, but the available type of monomers is still scant. Herein, two novel imine-linked COFs (TaDAP and TaDA) were constructed by the condensation of 1,3,5-tris-(4-aminophenyl) triazine with 2,6-diformylpyridine and 1,3-benzenedialdehyde under solvothermal conditions, respectively. And their structures were confirmed and characterized by solid state ^{13}C NMR, FT-IR, PXRD, TGA, SEM, TEM and nitrogen sorption isotherms. They appear as regular spherical particles and possess excellent thermal stability. It was also found that their dispersions emit strong fluorescence and display quick response to certain metal ions. Particularly, TaDAP can detect Fe^{3+} with sensitivity and selectivity. Moreover, two COFs both present excellent catalytic performance to Knoevenagel reaction. Accordingly, this work not only provides a new way to enrich the family of COFs, but also develops their potential applications in metal ions detection.

Introduction

Covalent organic frameworks (COFs) are a novel class of crystalline organic porous materials constructed from organic building blocks *via* reversible covalent bond formation. Generally, some reversible condensation reactions such as trimerization of nitriles,[1-3] boronic acid trimerization,[3,5] boronate ester formation[6-9] and Schiff base formation[10,11] are all effective tools to build COFs. Meanwhile, this kind of materials has shown promising applications in many fields, including chemical sensors, drug delivery and gas storage by virtue of their good thermal stability, low density and large specific surface area.[12-21]

However, depending on the requirement of specific geometries and rigid structures of building blocks, the type of monomers available to construct COFs is still scant. As a result, the reported pore patterns are mainly limited to triangular, quadrangular or hexagonal, which severely restricts the further development of COFs.[22-25] For example, the construction of COFs with hexagonal pores mostly depends on the condensation of C_3-symmetrical monomers and C_2-symmetrical monomers with two reactive groups in the opposite position strictly. Whereas, these severe requirements greatly reduce the range of monomers to be chosen. Thus, we try to introduce some new building blocks bearing two reactive groups in the meta-position into the frameworks. It could break through the previous ideas that the two functional groups of C_2-symmetrical monomers must be located in the opposite position, which is significant for broadening the optional range of monomers and developing COFs quickly.

Recently, several COFs were reported to kick in catalysis field and a number of reactions have been successfully catalyzed by COFs.[26-29] Nevertheless, most of them were used only as carriers, which showed little advantage over traditional supports. Wang and co-workers reported a novel catalyst of Pd loaded on imine-linked COF-LZU1, which exhibited excellent catalytic performance for Suzuki-Miyaura cross-coupling reaction in 96-98% yields for broad scope of substrates.[30] Phosphine-stabilized Pd nanoparticles supported on silica ($PdNP@PPh_2–SiO_2$) reported by Pankaj Das also enhanced the above reaction in 98% yield.[31] Actually, by means of a bottom-up or post-modified strategy, catalytic component can be introduced into COF catalysts. In fact, a few reports demonstrated that metal-free COFs can facilitate some specific reactions. A series of 3D COFs comprising both acidic and basic sites were exactly demonstrated to be excellent bifunctional catalysts for one-pot cascade reactions.[32] Given this, we plan to integrate the functional groups into framework to impart the as-prepared COFs themselves catalytic activity. Instead of only being supports, they can be constructed as Schiff base for some base-catalyzed reactions. At the same time, the basicity of COFs can be easily regulated by the introduction of pyridine unit, thereby affecting the catalytic activity of materials.

Therefore, two novel imine-linked COFs named TaDAP and TaDA were designed and synthesized by the condensation of 1,3,5-tris-(4-aminophenyl) triazine (TAPT) with 2,6-diformylpyridine (DAP) and 1,3-benzenedialdehyde (DA) under solvothermal conditions in this work, respectively. Their

[a] School of Chemical Engineering and Technology, Tianjin University, Tianjin 300350, People's Republic of China.
[b] Collaborative Innovation Center of Chemical Science and Engineering (Tianjin), Tianjin 300072, PR China
[c] Tianjin Engineering Research Center of Functional Fine Chemicals, Tianjin 300072, People's Republic of China
* Corresponding Author: lgchen@tju.edu.cn.
[1] These authors contributed equally to this work.
† Electronic supplementary information (ESI) available: Synthesis of monomers, TGA, UV-Vis absorption spectra of TaDAP and metal ions, and PXRD and simulated stacking modes of TaDA.

View Article Online
DOI: 10.1039/C8TA12417A

structures were confirmed and characterized by powder X-ray diffraction (PXRD) analysis with structural simulation, Fourier transform infrared (FT-IR) spectroscopy, solid-state ^{13}C cross-polarization/magic-angle spinning (CP/MAS) NMR spectroscopy, scanning electron microscopy (SEM), transmission electron microscopy (TEM) and nitrogen sorption isotherms. Furthermore, two COFs were applied to the metal ion detection and Knoevenagel condensation catalysis. TaDAP was found to be an excellent probe for the detection Fe^{3+} with selectivity and sensitivity. TaDA behaved as an effective catalyst for Knoevenagel reaction.

Experimental section

Materials

All reagents and solvents were purchased from the chemical suppliers (Jiangtian, Aladdin and Yuanli Chemical Reagent Co., Ltd) and used without further purification.

Synthesis

Synthesis of TaDAP 1,3,5-Tris-(4-aminophenyl) triazine (141.6 mg, 0.4 mmol), 2,6-diformylpyridine (81.1 mg, 0.6 mmol), 3M acetic acid (0.5 mL) and mesitylene/1,4-dioxane (1.5 mL,1/1 v/v) were added to a 10mL Pyrex tube. After being degassed via three freeze-pump-thaw cycles, the tube was sealed and then put into an oven at 120 °C for 5 days to yield a light-brown precipitate, which was collected by centrifugation. After being washed with acetone and dichloromethane three times and dried in vacuum at 120 °C for 12h, the final COF named TaDAP was obtained.

Synthesis of TaDA 1,3,5-Tris-(4-aminophenyl) triazine (141.6 mg, 0.4 mmol), 1,3-benzenedialdehyde (80.5 mg, 0.6 mmol), 3M acetic acid (0.5 mL) and mesitylene/1,4-dioxane (1.5 mL,1/1 v/v) were added to a 10mL Pyrex tube. After being degassed via three freeze-pump-thaw cycles, the tube was sealed and then put into an oven at 120 °C for 5 days to yield a bright-yellow precipitate, which was collected by centrifugation. After being washed with acetone and dichloromethane three times and dried in vacuum at 120 °C for 12h, the final COF named TaDA was obtained.

Chemical and physical characterization

^1H NMR spectra were recorded on a Bruker Avance III 400 MHz spectrometer using tetramethylsilane as an internal standard. Fourier transform infrared spectra (FT-IR) were collected on a Nicolet 22 AVATAR 370 FT-IR spectrometer in the 4000-550 cm-1 region. ^{13}C CP MAS NMR spectra were recorded on a Infinityplus 300 MHz solid state NMR spectrometer. Nitrogen adsorption-desorption isotherms were measured at 77 K with a NOVA 2000e surface and porosity analyzer (Quantachrome, US). Thermogravimetric analysis (TGA) was performed on an STA 409 PC thermal analyzer at a heating rate of 10 °C/min from room temperature to 700 °C. X-ray diffraction (XRD) patterns were recorded on a Rigaku D/max 2500 X-ray diffractometer using a CuKα radiation source (40 kV, 100 mA) in the range of 1.5-30°. Transmission electron microscopy (TEM) was performed on a FEI Tecnai G2 F20 electron microscope operated at an accelerating voltage of 200 kV. Sample was prepared by dropping a sonicated ethanol solution of the COFs over a carbon-coated copper grid. Scanning electron microscopy (SEM) images were obtained with a FEI Nanosem 430 scanning electron microscope. UV–Vis absorption spectra were measured on an L8 spectrophotometer. Fluorescence spectra were recorded on Hitachi F-2500 fluorescence spectrophotometer. Geometry optimization and structural simulation was performed at Material Studio 7.0.

Results and discussion

Structure and chemical composition of the COFs

TaDAP and TaDA were synthesized by the condensation of 1,3,5-tris-(4-aminophenyl) triazine with 2,6-diformylpyridine and 1,3-benzenedialdehyde under solvothermal conditions, respectively. Their structures were confirmed by FT-IR and solid state ^{13}C CP/MAS NMR spectroscopy. As shown in Fig. 1a, two strong adsorption bands were observed at 1504 and 1365 cm^{-1} in TaDA and TaDAP's spectra, indicating the presence of triazine ring. Compared with the spectrum of TAPT, the N-H stretching bands (3209, 3323, and 3460 cm^{-1}) have totally disappeared in their spectra, implying the complete consumption of the starting material TAPT. Similarly, the peaks at 1718 cm^{-1} and 1695 cm^{-1} (C=O stretching) occurring in the spectra of other two monomers (DAP and DA) also disappeared in the spectra of TaDAP and TaDA. Meanwhile, new stretching peaks at 1641 cm^{-1} for TaDAP and 1623cm^{-1} for TaDA were observed, indicating the formation of imine linkages. More information was obtained by ^{13}C CP/MAS NMR analysis. From Fig. 1b, the peaks at 158.6 and 159.2 ppm were assigned to the carbon atoms of imine groups, as well as the low-field peaks at about 169.5 and 169.4 ppm can be ascribed to the triazine ring for TaDPA and TaDA, respectively. Moreover, the absence of the signal for the formyl carbons of DAP and DA around 190 ppm illustrates that they have been completely converted to Schiff base. These results are consistent with FT-IR.

The morphologies of TaDAP and TaDA were examined using SEM and TEM. As can be seen from SEM images (Fig. 2a and 2b), the monomers of TaDAP and TaDA self-assemble to form spherical agglomerates with inhomogeneous diameters of 0.5~1.1 μm, which is approximately consistent with TEM images (Fig. 2c and 2d). And this kind of morphology is also similar to some reported COFs.[33-35] However, the spherical surface of TaDA is smoother than that of TaDAP observed from TEM. In

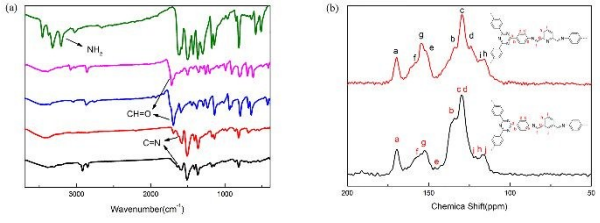

Fig.1 (a) FT-IR spectral of 1,3,5-Tris-(4-aminophenyl) triazine (green line), 2,6-diformylpyridine (purple line), 1,3-benzenedialdehyde (blue line), TaDA (red line) and TaDAP (black line); (b) Solid state ^{13}C cross-polarization magic-angel spinning NMR spectrum of TaDAP (red line) and TaDA (black line).

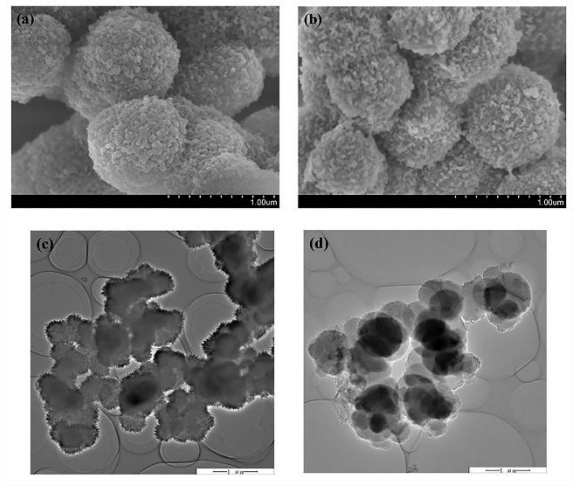

Fig.2 SEM images of TaDAP (a) and TaDA (b); TEM images of TaDAP (c) and TaDA (d).

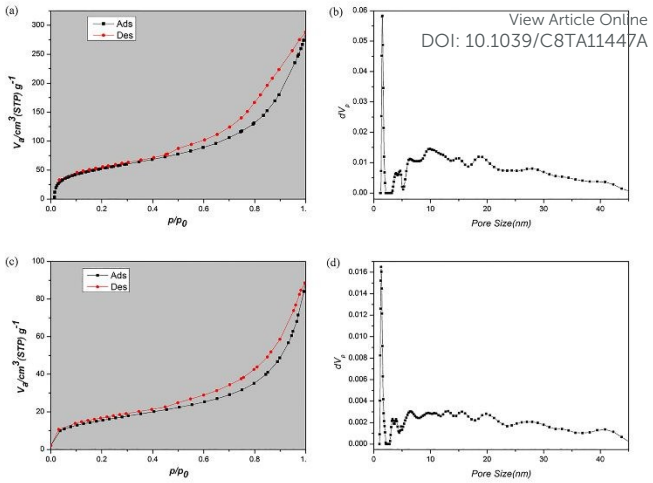

Fig.3 N_2 adsorption/desorption isotherms for TaDAP (a) and TaDA (c); pore size distributions for TaDAP (b) and TaDA (d).

addition, thermogravimetric analysis (TGA) was carried out on the dry COFs samples under a nitrogen atmosphere (Fig. S1) and it reveals that they are stable up to 500 °C for both TaDAP and TaDA.

The specific surface areas and porous structures of TaDAP and TaDA were determined using the nitrogen sorption isotherms at 77 K. As shown in Fig. 3a and 3c, TaDAP and TaDA exhibit typical type IV isotherms. The rapid uptake at a low relative pressure confirms their permanent microporosity. The appearance of a hysteresis loop above P/P_0=0.45 and the sharp increase above P/P_0=0.8 indicate the presence of mesopores or even macropores, which was presumably caused by the voids in the loose stacking layered-material. The Brunauer–Emmett–Teller (BET) surface areas of TaDAP and TaDA were calculated to be 197.3 and 57.1 $m^2\,g^{-1}$, respectively. The total pore volumes were 0.27 $cm^3\,g^{-1}$ for TaDAP and 0.08 $cm^3\,g^{-1}$ for TaDA at P/P_0=0.99. It is supposed that the introduction of pyridine unit changes the combined mode of monomers for TaDAP. It makes the surface of formed spherical particles rougher, which may lead to larger surface area and pore volumes. On the basis of the density functional theory (DFT), the pore size distributions of TaDAP and TaDA were estimated, which mainly distributed around 1.54 nm and 1.30 nm, separately (Fig. 3b and 3d).

The crystal structures of TaDAP and TaDA were determined by PXRD analysis coupled with structural simulation. As can be seen from the comparative PXRD patterns of TaDAP and TaDA (Fig. 4a), the peak positions of these two samples are similar. Concretely, the experimental PXRD pattern of TaDAP appears a strong peak at 5.29°, along with other relatively weak peaks at 3.31°, 11.45°, 15.78° and 19.86°. Meanwhile, a broad peak at 26.06° that is attributed to π-π stacking between TaDAP layers is also observed. Similarly, the observed PXRD pattern of TaDA exhibits six peaks at 3.07°, 5.09°, 11.20°, 15.54°, 19.54° and 25.58°, respectively. And the interlayer spacings are 3.33 Å for TaDAP and 3.39 Å for TaDA. According to previous work, modifications to the electronic structure of COF monomers can change the π-π stacking between the layers, which further resulting in the difference of crystallinity or even morphology.[36-38] Therefore, it is speculated that the existence of pyridine N affects the structural properties here. Moreover, the structural simulation of the AA-stacking and AB-stacking modes were operated for these two samples (Fig. S2a, S2b, S2e and S2f). However, neither heart-shaped eclipsed AA-stacking mode nor petal-shaped staggered AB-stacking mode can reproduce the experimentally observed PXRD data absolutely, which is likely that the building units bearing formyl groups are bent structures with the certain angle, inducing defects during the crystallization of two samples and lowering the symmetry of these materials.[39] To find a mode that can match experimental data better, some other possible stacking modes were also simulated (Additional cif documents). Take TaDAP as an example, after geometrical energy minimization by the universal force field, the unit cell was built using space group P3 with the optimized parameters of a = b = 33.52 Å and c = 3.50 Å, α = β = 90°, and γ = 120°. Then, by adjusting the relative position of interlayers, the most probable structure was obtained (Fig. 4c and 4d). Furthermore, Pawley refinement was carried out to afford the refined PXRD patterns with the unit cell parameters a = 34.33 Å, b = 33.89 Å and c = 3.66 Å, α = 91.44°, β = 91.18°, and γ = 121.57° (R_p = 5.29% and R_{wp} = 7.96%). The refined XRD pattern was in good agreement with the experimental profile, as was evident by their negligible difference (Fig. 4b).

Fluorescent performance of the COFs

As mentioned above, two novel imine-linked COFs were successfully synthesized. Occasionally, it was found that the dispersions of TaDAP and TaDA could emit fluorescence, so the UV-vis absorption and fluorescence spectra were recorded. Compared with most of the reported 2D COFs that cannot emit fluorescence, the two COFs in our work were connected by non-linear 2-c linkers. The special linkers can be twisted to some extent, resulting in the loose stacking and weak π-π

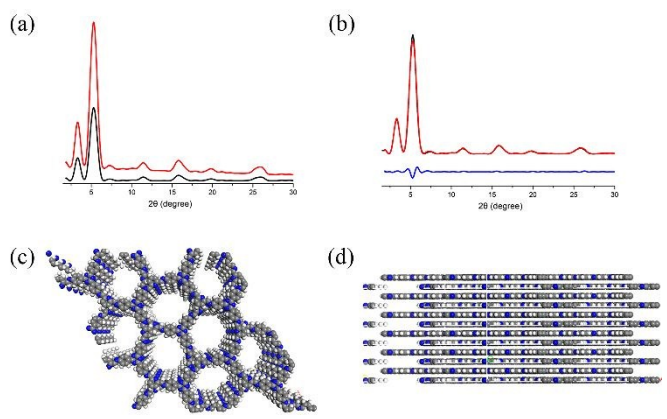

Fig.4 (a) PXRD profiles of TaDA (red line) and TaDAP (black line); (b) Observed PXRD pattern (red, the major reflections are assigned) and refined modeling profile (black) of TaDAP; (c) Optimal simulated mode and (d) side view of TaDAP (grey, carbon; white, hydrogen; blue, nitrogen).

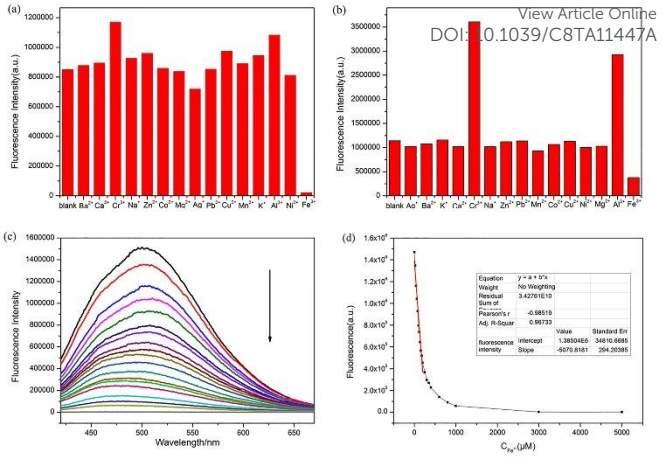

Fig.5 Effect of metal ions (1.0 mM each) on the fluorescence of TaDAP (a) and TaDA (b) in the DMF/H_2O (9:1, v/v); (c) Fluorescence spectra of TaDAP in DMF/ H_2O (9:1, v/v) upon addition of Fe^{3+} (from 0.02 mM to 0.86 mM); (d) Fluorescence intensity of TaDAP at 507nm as a function of different concentrations of Fe^{3+} in the DMF/H_2O (9:1, v/v). λ_{ex}=355 nm.

interaction between the layers, which avoids the fluorescence quenching of the materials. Furthermore, the amorphous components corresponding to the two COFs have been prepared and their fluorescence spectra have been examined (Fig. S4 and Fig. S5). It was found that the maximum fluorescence emission wavelength of the corresponding amorphous components is blue-shifted and the maximum fluorescence emission intensity is enhanced compared with those of the two COFs, which indicates that there exist certain conjugated structures and partial π-π interaction in the two COFs but the effect is not enough to quench the fluorescence completely. Subsequently, based on their spectra, we try to explore if they have a fluorescent response to different metal ions. As shown in Fig. 5a, only when adding Fe^{3+}, the fluorescence of TaDAP dispersion significantly quenched, while it changed negligibly with addition of other metal ions. This indicates that TaDAP shows excellent selectivity towards Fe^{3+}. Thus, the sensitivity of TaDAP for Fe^{3+} was systematically examined. With the incremental concentration of Fe^{3+}, the fluorescence intensity of TaDAP decreased gradually (Fig. 5c). As can be seen from Fig. 5d, a good linear relationship between the fluorescence intensity and the concentration of Fe^{3+} was obtained in the range of 0.02–0.2 mM, which made it possible to be used in the quantitative detection of Fe^{3+}. The limit of detection (LOD) for Fe^{3+} was calculated to be 18 μM. The response mechanism of TaDAP was also studied and it turns out that the absorption competition quenching (ACQ) mechanism for sensing Fe^{3+} is applicable (Fig. S7). The UV-vis absorption spectra of all these metal ions were recorded, but it was found that only Fe^{3+} had a significant absorption peak at 360 nm. Then we further compared the UV-vis absorption spectrum of TaDAP with that of Fe^{3+}. As a result, there is an obvious overlap between the spectroscopies of Fe^{3+} and TaDAP, indicating that there is an absorption competition quenching effect between them. In other words, since Fe^{3+} has larger molar extinction coefficient than TaDAP, most of photons from the light source was absorbed by Fe^{3+}, resulting in the proportion of photons absorbed by TaDAP decreased. And the quantity of the excited electrons in TaDAP reduced so that the fluorescence of TaDAP quenched.[40] However, the same measurement was conducted on TaDA and it was found that the fluorescence of TaDA had a response to not only Fe^{3+} but also other trivalent metal ions (Fig. 5b). Particularly, when adding Cr^{3+} and Al^{3+} to the medium, the fluorescence intensity of TaDA increased obviously. This characteristic makes it potential to the detection of trivalent metal ions. According to the comparative PXRD patterns of TaDA before and after being treated with Al^{3+} and Cr^{3+} (Fig. S8), it was found that the interaction between TaDA and Al^{3+} or Cr^{3+} might lead to the structural change of TaDA, further resulting in the enhancement of fluorescence.

Catalytic performance of the COFs

Afterwards, the catalytic activity of TaDAP and TaDA was examined by Knoevenagel condensation (Scheme 1), which is a classical base-catalyzed reaction.[41] It was found that the above Knoevenagel reaction proceeded effectively to yield the corresponding products upon TaDAP or TaDA, while the blank experiment without the catalyst afforded a negligible of benzaldehyde. Specifically, the conversion of benzaldehyde increased to 56.8% over TaDAP and further reached up to 68.9% in the case of TaDA as a catalyst. To explore the catalytic mechanism, the activity of monomers was evaluated firstly. It indicates that 1,3,5-tris-(4-aminophenyl) triazine (TAPT) as a homogeneous catalyst showed better catalytic activity than two COFs, while 2,6-diformylpyridine (DAP) and 1,3-benzenedialdehyde(DA) exhibited poor catalytic performance (Table S1). In turn, it further demonstrates that the imine or the terminal amino groups rather than the pyridine groups play the catalytic role in this reaction. Verified by a control experiment and considering that imine groups widely exist in the skeleton of the two COFs while the terminal amino groups are very limited, the imine groups are identified as the main active sites.[42-46] Then, the molecular sizes of the reactants and products were

View Article Online DOI: 10.1039/C8TA11457A

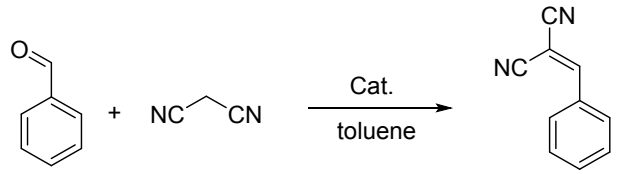

Scheme 1. Knoevenagel condensation reaction between benzaldehyde and malononitrile.

measured and compared with the pore sizes of the two COFs to explore whether the porosity has an influence on the catalytic activity (Table S2). But the results showed that the pore size might not be the main factor to the catalytic activity. Indeed, due to the specialty of the two COFs structures, the combined effects of specific surface area, porosity and other possible factors may all contribute to the catalytic activity, so further research on this issue will be done more carefully in the future work. Subsequently, the reaction conditions were optimized using TaDA as a catalyst (Table 1). As can be seen from the results summarized in Table 1, temperature is the key parameter. Finally, under the optimal experimental conditions, a satisfactory conversion of benzaldehyde (97.7%) was achieved.

Table 1

Optimization of reaction conditions using TaDA as base catalyst for the reaction of benzaldehyde and malononitrile.[a]

T /°C	Cat. /mg	t /h	Con. /%
90	0	8	-
50	10	8	27.9
70	10	8	48.3
90	10	8	68.9
110	10	8	81.4
100	10	8	86.3
100	20	8	100
100	15	8	94.3
100	15	6	83.0
100	15	10	95.3
100	15	12	97.7

[a] Reaction conditions: benzaldehyde (2 mmol), malononitrile (2 mmol), toluene (2 mL), temperature, time and TaDA.

[b] Conversion was determined by GC and selectivity was always more than 99% of the condensed product in all the cases.

Conclusion

In summary, two novel imine-linked COFs have been successfully synthesized by introducing bent building units under solvothermal conditions and their chemical structures were confirmed by FT-IR and solid state ^{13}C CP/MAS NMR spectroscopy. From PXRD patterns, their crystal structure is similar but the crystallinity of TaDA is higher than TaDAP. Based on TG analysis, it reveals that they have high thermal stability. And verified by electron microscopy images, both materials appear as spherical agglomerates. Besides, they both possess microporous and mesoporous feature but the surface area is truly different according to N_2 sorption isotherms. Moreover, it was found that their dispersions emit strong fluorescence and display quick response to certain metal ions, especially TaDAP can be employed to detect Fe^{3+} with sensitivity and selectivity. Meanwhile, two COFs both present excellent catalytic performance to Knoevenagel reaction. It is satisfying that the conversion of benzaldehyde can be up to 100% and the selectivity of condensed product can be more than 99% using TaDA as a catalyst. Also, a deeper study of catalytic mechanism should be done in the future work. Thus, this work not only provides a new synthetic idea towards the complement of COF materials, but also develops their potential applications.

Conflicts of interest

There are no conflicts to declare.

Acknowledgements

Financial support was provided by the National Natural Science Foundation of China (Grant No. 21808161 and 21576194).

References

1 J. Roeser, K. Kailasam and P. A. Thomas, Chemsuschem, 2012, 5, 1793-1799.
2 L. Hao, J. Ning, B. Luo, B. Wang, Y. Zhang, Z. Tang, J. Yang, A. Thomas and L. Zhi, Journal of the American Chemical Society, 2015, 137, 219-225.
3 B. Onur, H. J. Sang, N. T. Siddulu, K. Daeok and C. Ali, Acs Applied Materials & Interfaces, 2017, 9, 7209-7216.
4 D. N. Bunck and W. R. Dichtel, Angewandte Chemie, 2012, 124, 1921-1925.
5 H. M. Elkaderi, J. R. Hunt, J. L. Mendozacortés, A. P. Côté, R. E. Taylor, M. O'Keeffe and O. M. Yaghi, Science, 2007, 316, 268-272.
6 S. Wan, J. Guo, J. Kim, H. Ihee and D. Jiang, Angewandte Chemie, 2010, 121, 3253-3253.
7 L. Chen, K. Furukawa, J. Gao, A. Nagai, T. Nakamura, Y. Dong and D. Jiang, Journal of the American Chemical Society, 2014, 136, 9806-9809.
8 K. Duan, J. Wang, Y. T. Zhang and J. D. Liu, Journal of Membrane Science, 2019, 572, 588-595.
9 D. D. Medina, J. M. Rotter, Y. Hu, M. Dogru, V. Werner, F. Auras, J. T. Markiewicz, P. Knochel and T. Bein, Journal of the American Chemical Society, 2015, 137, 1016-1019.
10 M. Mu, Y. Wang, Y. Qin, X. Yan, Y. Li and L. Chen, Acs Applied Materials & Interfaces, 2017, 9, 22856.
11 T.-Y. Zhou, S.-Q. Xu, Q. Wen, Z.-F. Pang and X. Zhao, Journal of the American Chemical Society, 2014, 136, 15885-15888.
12 S. Y. Ding, M. Dong, Y. W. Wang, Y. T. Chen, H. Z. Wang, C. Y. Su and W. Wang, Journal of the American Chemical Society, 2016, 138, 3031.
13 F. M. E. Ahmed, H. K. Cheng, A. Abdulmohsen, Y. Christine, Y. Yusuke, K. Jeonghun and W. K. Shiao, Journal of Materials Chemistry A, 2018, 6, 19532.
14 G. Lin, H. Ding, D. Yuan, B. Wang and C. Wang, Journal of the American Chemical Society, 2016, 138, 3302-3305.
15 Y. Zeng, R. Zou and Y. Zhao, Advanced Materials, 2016, 28, 2855-2873.
16 N. Huang, R. Krishna and D. Jiang, Journal of the American Chemical Society, 2015, 137, 7079-7082.
17 S. Lin, C. S. Diercks, Y. B. Zhang, N. Kornienko, E. M. Nichols, Y. Zhao, A. R. Paris, D. Kim, P. Yang and O. M. Yaghi, Science, 2015, 349, 1208-1213.

18 X. Wang, X. Han, J. Zhang, X. Wu, Y. Liu and Y. Cui, Journal of the American Chemical Society, 2016, 138, 12332-12335.
19 H. S. Xu, S. Y. Ding, W. K. An, H. Wu and W. Wang, Journal of the American Chemical Society, 2016, 138, 11489-11492.
20 Q. Fang, J. Wang, S. Gu, R. B. Kaspar, Z. Zhuang, J. Zheng, H. Guo, S. Qiu and Y. Yan, Journal of the American Chemical Society, 2015, 137, 8352-8355.
21 V. S. Vyas, M. Vishwakarma, I. Moudrakovski, F. Haase, G. Savasci, C. Ochsenfeld, J. P. Spatz and B. V. Lotsch, Advanced Materials, 2016, 28, 8749.
22 S. Dalapati, S. Jin, J. Gao, Y. Xu, A. Nagai and D. Jiang, Journal of the American Chemical Society, 2017, 135, 17310-17313.
23 G. Das, B. P. Biswal, S. Kandambeth, V. Venkatesh, G. Kaur, M. Addicoat, T. Heine, S. Verma and R. Banerjee, Chemical Science, 2015, 6, 3931-3939.
24 S. Q. Xu, T. G. Zhan, Q. Wen, Z. F. Pang and X. Zhao, Acs Macro Letters, 2016, 5, 99-102.
25 S. Dalapati, M. Addicoat, S. Jin, T. Sakurai, J. Gao, H. Xu, S. Irle, S. Seki and D. Jiang, Nature Communications, 2015, 6, 7786.
26 H. Xu, J. Gao and D. Jiang, Nature Chemistry, 2015, 7, 905.
27 L. H. Li, X. L. Feng, X. H. Cui, Y. X. Ma, S. Y. Ding and W. Wang, Journal of the American Chemical Society, 2017, 139, 6042-6045.
28 Z. Jie, H. Xing, X. Wu, L. Yan and C. Yong, Journal of the American Chemical Society, 2017, 139.
29 H. Xing, Q. Xia, J. Huang, L. Yan, C. Tan and C. Yong, Journal of the American Chemical Society, 2017, 139, 8693.
30 D. SY, G. J, W. Q, Z. Y, S. WG, S. CY and W. W, Journal of the American Chemical Society, 2011, 133, 19816-19822.
31 D. Sahu and P. Das, Rsc Advances, 2015, 5, 3512-3520.
32 H. Li, Q. Pan, Y. Ma, X. Guan, M. Xue, Q. Fang, Y. Yan, V. Valtchev and S. Qiu, Journal of the American Chemical Society, 2016, 138, 14783-14788.
33 Q. Gao, X. Li, G.-H. Ning, K. Leng, B. Tian, C. Liu, W. Tang, H.-S. Xu and K. P. Loh, Chemical Communications, 2018, 54, 2349-2352.
34 C.-X. Yang, C. Liu, Y.-M. Cao and X.-P. Yan, Chemical Communications, 2015, 51, 12254-12257.
35 S. Kandambeth, V. Venkatesh, D. B. Shinde, S. Kumari, A. Halder, S. Verma and R. Banerjee, Nature Communications, 2015, 6.
36 A. Halder, S. Kandambeth, B. P. Biswal, G. Kaur, N. C. Roy, M. Addicoat, J. K. Salunke, S. Banerjee, K. Vanka, T. Heine, S. Verma and R. Banerjee, Angewandte Chemie-International Edition, 2016, 55, 7806-7810.
37 S. B. Alahakoon, G. T. McCandless, A. A. K. Karunathilake, C. M. Thompson and R. A. Smaldone, Chemistry-a European Journal, 2017, 23, 4255-4259.
38 X. Chen, M. Addicoat, S. Irle, A. Nagai and D. Jiang, Journal of the American Chemical Society, 2013, 135, 546-549.
39 G. H. V. Bertrand, V. K. Michaelis, T.-C. Ong, R. G. Griffin and M. Dinca, Proceedings of the National Academy of Sciences of the United States of America, 2013, 110, 4923-4928.
40 M. Wang, H. Zhang, L. Guo and D. Cao, Sensors and Actuators B-Chemical, 2018, 274, 102-109.
41 Y. Luan, Y. Qi, H. Gao, R. S. Andriamitantsoa, N. Zheng and G. Wang, Journal of Materials Chemistry A, 2015, 3, 17320-17331.
42 A. U. Katherine and J. M. Duncan, New Journal of Chemistry, 2000, 24, 591-595.
43 H. Li, Q. Pan, Y. Ma, X. Guan, M. Xue, Q. Fang and Y. Yan, Journal of the American Chemical Society, 2016, 138, 14783-14788.
44 Q. Fang, S. Gu, J. Zheng, Z. Zhuang, S. Qiu and Y. Yan, Angewandte Chemie-International Edition, 2014, 53, 2878-2882.
45 M. Zhang, P. Zhao, Y. Leng, G. Chen, J. Wang and J. Huang, Chemistry-A European Journal, 2012, 18, 12773-12782.
46 R. Jangir, A. C. Kalita, D. Kaleeswaran, S. K. Gupta and R. Murungavel, Chemistry-A European Journal, 2018, 24, 6178-6190.

View Article Online
DOI: 10.1039/C8TA11447A

View Article Online
DOI: 10.1039/C8TA11447A

Two novel COFs using nonlinear C_2-linkers are constructed and perform excellent property for metal ion detection and Knoevenagel condensation catalysis.